BNL-80171-2008-JA

REPLACING PIXEL REPRESENTATIONS BY POINT-FUNCTION SCHEMES FOR REDUCING DISCRETIZATION ERROR IN ILL-POSED REMOTE SENSING PROBLEMS, WITH EXAMPLES FROM CLOUD TOMOGRAPHY

Dong Huang[1], Yangang Liu[1], and Warren Wiscombe[1,2]

[1]Brookhaven National Laboratory, Upton, NY 11973, U.S.A.
[2]NASA Goddard Space Flight Center (code 913), Greenbelt, MD 20771, U.S.A.

April 2008

Submitted for publication in
IEEE Geoscience and Remote Sensing Letters

Corresponding Author: Dong Huang, Environmental Sciences Department, Brookhaven National Laboratory, 75 Rutherford Dr., Upton, NY 11973; Telephone: (631) 344-5818; Email: dhuang@bnl.gov

Environmental Sciences Department/Atmospheric Sciences Division

Brookhaven National Laboratory
P.O. Box 5000
Upton, NY 11973-5000
www.bnl.gov

DISCLAIMER

Abstract

Because of their simplicity and low computational cost, discretizations based on pixels have held sway in remote sensing since its inception. Yet functional representations are clearly superior in many applications, for example when combining retrievals from dissimilar remote sensing instruments. Here, using cloud tomography as an example, we show that a point-function discretization scheme based on linear interpolation can reduce retrieval error up to 40% compared to a conventional pixel scheme. This improvement is particularly marked because cloud tomography, like the vast majority of remote sensing problems, is ill-posed and thus a small inaccuracy, such as discretization error, can cause a large error in the retrievals.

1. Introduction

Discretizations based on pixels have held sway in remote sensing since its inception. They have shown many disadvantages as earth observations are relying more and more on multi-sensor data (a single instrument usually does not convey enough information to accurately retrieve the desired parameters). For example, the NASA EOS A-train satellites carrying many dissimilar sensors (active vs. passive, different instantaneous field of view, etc.) have provided unprecedented data for comprehensive studies of Earth weather and climate (Stephens et al., 2002). In the pixel framework, the mismatch of pixel sizes used in various satellite products poses many challenges for data integration. Another example is using multiple ground instruments to measure atmospheric properties, e.g., a microwave radiometer and a radar with different antenna beam widths. The dissimilar ground instruments actually view cones of different apex angles; thus rectangular pixels are not a natural match to the cones and unavoidably introduce some artifacts.

Furthermore, the inverse problems of remote sensing are often ill-posed, making the retrieval sensitive to small inaccuracies such as discretization errors. The discretization errors will be magnified in the numerical inversion procedure, making the retrieval even more inaccurate (Bockman, 2000). Superficially, it would seem that discretization error could be reduced by using smaller grids/pixels, but in practice this may not improve the retrieval. This is because finer grids lead to a larger number of unknowns, thus a higher dimension in the involved inverse problem, which in turn makes the inverse problem more ill-posed and thus the retrieval more sensitive to perturbations (Hansen, 1998). The tradeoff between discretization and ill-posedness limits the ability of

remote sensing techniques to resolve the desired variables at small spatial scales. The interweaving issue of ill-posedness and discretization needs to be addressed in order to improve the retrieval.

Functional representations would work better for the above issues than the widely used pixel scheme. With a functional representation, satellite images can be sampled at any resolution and thus can overcome the problem of resolution mismatch between different satellite products. Although regularization techniques using *a priori* knowledge of the retrieval can reduce the retrieval sensitivity to perturbations (Twomey, 1977), functional representations can further help the interweaving issue of ill-posedness and discretization. The variable to be retrieved is expressed as a superposition of some prescribed basis functions (usually orthogonal empirical functions derived from historical measurements, or functions such as the Fourier basis and polynomials). Then the only unknowns are the coefficients for each basis function; in this way the discretization error can be reduced without increasing the dimension of the retrieval problem.

Unfortunately, the measurements needed to specify the basis functions empirically are unavailable in many applications. And familiar but arbitrary basis functions like the Fourier set may be inappropriate. The objective of this paper is to develop a functional discretization scheme, called point-function discretization, through which a continuous variable is approximated by interpolating over the whole domain based on a set of point values. Microwave cloud tomography is then used as an example to show that the point-function discretization scheme can be integrated into a regularization algorithm to reduce the discretization error and thus improve the retrieval.

2. Pixel and point-function representations

Remote sensing retrieval problems can generally be formulated as: *deriving the distribution of some desired variable* $x(r)$ *within a domain* Ω *from the set of remote sensing measurements* $\{b_i\}$. In many applications, the problem can be reduced to solving a set of Fredholm integral equations of the first kind:

$$\int_{r\in\Omega} a_i(r)x(r)dr = b_i, \tag{1}$$

where $a_i(r)$ is a kernel function representing the forward operator that relates the desired variable $x(r)$ to the measurements $\{b_i\}$.

We partition the spatial domain Ω into N non-overlapping elements E_i such that $\bigcup_{i=1}^{N} E_i \equiv \Omega$. The elements join at n vertex nodes e^j, j=1, …, n (a node is a point at which three or more elements intersect). For simplicity, throughout this study we use equal-sized square elements so that the nodes are equally spaced by a distance d. The solution $x(r)$ to Eq. (1) is approximated by a superposition of a set of predefined basis functions $w(r, e^j)$:

$$x(r) \approx \sum_{j=1}^{n} w(r,e^j)x(e^j). \tag{2}$$

The inverse problem now is to find the nodal values $x(e^j)$ from which the solution everywhere in the domain Ω can be derived by the interpolation rule (2).

Different choices of the basis functions lead to different discretization models. This is illustrated as follows. Let e^j be the nearest node to an arbitrary location r. Setting the basis to be the Kronecker delta function, i.e., $w(r, e^i)=w(e^j, e^i)=\delta_{ij}$, assures that $x(r)$ takes the same value in the box of size d centered at e_j. Hence choosing the Kronecker delta function as the basis coincides with the conventional pixel scheme.

Replacing the Kronecker delta function with localized linear interpolation functions, we get our point-function discretization model. Let (r_x, r_y) and (e^i_x, e^i_y) denote the coordinates of point r and node e^i in the two-dimensional case, we define the basis function as the bi-linear interpolation function:

$$w(r, e^i) \equiv (1-t)(1-u)\,, \tag{3}$$

where $e^i_x \le r_x \le e^i_x + d$ and $e^i_y \le r_y \le e^i_y + d$, and

$t \equiv (r_x - e^i_x)/d$

$u \equiv (r_y - e^i_y)/d$.

We call the basis function defined by Eq. (3) "the pyramid basis" because it actually looks like a pyramid when plotted in the three-dimensional space.

With the basis functions specified by Eq. (3), substituting Eq. (2) into in Eq. (1) leads to:

$$\sum_{j=1}^{n} x(e_j) \int_{r \in \Omega} a_i(r) w(r, e_j) dr = b_i \tag{4}$$

Rewrite Eq. (4) as a matrix equation:

$$\mathbf{Ax} = \mathbf{b}, \tag{5}$$

where $\mathbf{A} \equiv (a_{ij})$ is an *m* x *n* kernel matrix representing the forward operator and its elements are $a_{ij} = \int_{r \in \Omega} a_i(r) w(r, e_j) dr$; $\mathbf{x} \equiv \left(x(e_1), x(e_2), \cdots, x(e_n)\right)^T$ is the vector of desired variables at the *n* nodes; and $\mathbf{b} \equiv \left(b_1, b_2, \cdots, b_m\right)^T$ is the vector of remote sensing measurements. Hereby, the retrieval problem now reduces to solving the matrix equation (5) for a set of point values and then interpolating the point values for the desired variables in the entire domain.

3. Application to microwave cloud tomography

3.1 Cloud tomography and modified DSCNNLS

Cloud tomography is a method for retrieving 3D distributions of the cloud liquid water content (LWC) from radiometric data (Warner et al., 1985; Warner and Drake, 1986; Twomey, 1987). This method involves measuring the microwave cloud emission from a multiplicity of different directions by a single airborne or several ground-based radiometers, and inverting the resulting radiometric data for the LWC distribution by numerical procedures. The tomographic retrieval problem is highly ill-posed especially when only a few ground-based radiometers are used, as shown in Huang et al.(2008a). Regularization techniques that use various types of prior knowledge to constrain the retrievals are necessary to reduce this sensitivity. The Double-side plus Smoothness Constrained Non-Negative Least Squares (DSCNNLS) algorithm capable of using

several types of constraints significantly improved the cloud tomography retrievals compared to the standard least squares method (Huang et al., 2008b).

The conventional pixel scheme, in conjunction with the ill-posedness of the retrieval problem, produces unfavorable artifacts in the tomographic retrievals (Scales et al., 1990; Delprat-Jannaud and Lailly, 1993). Operational microwave antennas do not have an infinitesimal beam width. As illustrated in Figure 1, four radiometer with different beam widths are actually viewing cones of different apex angles centered around the nominated rays. Considering the geometric mismatch, it is thus not surprising that dividing the retrieval space into rectangular boxes will introduce artifacts in the tomographic retrieval. Moreover, some rays graze a pixel through its corner such that the path lengths of these rays in this pixel are very small, and so carry little information about this pixel. This will directly result in artifacts in the retrieval.

To test the capability of the point-function discretization scheme, we select two very different cloud cases: a stratocumulus and a broken cumulus . Both cases are 5 km wide and 1.5 km high snapshots from a large eddy simulation model (Ackerman et al., 1995). Four simulated radiometers of 0.3 K noise level and 2-degree beam width are spaced equally along a line of 10 Km on the ground. Each radiometer scans the upper plane within 80^{o} elevation of zenith at an 0.35^{o} increment and this scanning strategy results in a total of 900 rays intersecting the 5 km by 1.5 km domain. The brightness temperature data for each ray are computed based on a radiative transfer equation and a prescribed antenna response function (Huang et al., 2008a).

Using Eqs. (2-5), we then replace the pixel discretization scheme implemented in the original DSCNNLS algorithm with the point-function discretization scheme to handle

the interweaving issue of ill-posedness and discretization. With its ability of using various constraints, the DSCNNLS algorithm enables us to improve the ill-conditioned kernel matrix and thus to better separate the discretization effect from the ill-posedness effect. The modified DSCNNLS algorithm is used to retrieve the LWC values on a set of 30 by 30 points from the simulated brightness temperatures . The resulting point values are then interpolated using Eq. (2) to obtain the cloud water distribution in the 5 km by 1.5 km domain.

3.2 Examination of discretization error and ill-posedness

Here, the capability of the pixel and point-function discretization schemes to approximate the true images is quantified by root mean squared (rms) error, computed by re-sampling the discretized image back to the resolution of the true image and then calculating the root mean squared pixel-wise difference between the two images. While the ill-posedness of the underlying problems is characterized by the condition number of the corresponding kernel matrix **A**, which is the ratio of the maximum to minimum singular values. Figure 2 shows an example of the true cloud images and the corresponding discretized images from the pixel and point-function discretization schemes using a total of 900 pixels or points. The point-function discretization scheme produces more realistic approximations than the conventional pixel scheme; the rms errors of the pixel and the point function schemes are 0.055 gm^{-3} and 0.025 gm^{-3} for the stratocumulus cloud, 0.067 gm^{-3} and 0.040 gm^{-3} for the broken cumulus cloud. Note that the discretized images are obtained by either aggregating the true images (for the pixel scheme) or minimizing the rms difference between the true and discretized images (for the point-function discretization scheme).

The accuracy of a discretized approximation to a continuous field depends on the smallest scale that the discretization scheme can resolve. This scale is usually determined by the total number of coefficients (pixels, points, or spectra) used in the discretization scheme. With the same number of coefficients, the point-function discretization scheme significantly better approximates the cloud images than the pixel scheme: the rms error of the point-function discretization scheme is about 60-80% of that of the pixel scheme (from 25 to 900 pixels or points); with less than 25 coefficients neither scheme works well while for more than 1600 pixels or points both schemes work well (Figure 3a). In contrast, the condition number of the pixel scheme agrees well with that of the point-function scheme in the whole spectrum (Figure 3b, very high order singular values would be numerically unstable and thus the condition numbers were not calculated when the number of pixels or points is more than 900). Note that a larger condition number means a more ill-posed retrieval problem. Furthermore, figure 3 reveals the mixed consequences of using finer discretization: the discretization error unsurprisingly decreases when more pixels or points are used (Figure 3a), while the condition number increases with finer discretization (Figure 3b). This confirms that discretization error and ill-posedness of the involved retrieval problem trade-off against each other and thus using finer discretization may not improve the retrievals.

3.3 Retrieving results

The reduction of discretization error by the point-function discretization scheme is expected to improve the retrieval as well. Figure 4 shows the true and retrieved LWC distributions for the two cloud cases obtained by using the pixel and point-function discretization schemes. Although the retrieved images using the pixel scheme reasonably

capture the spatial patterns of the original images, they surfer from some noticeable artifacts. For the first cloud case, some spurious cloud pieces appear below the cloud base and over the cloud top (Figure 4, the middle plate on the top). Furthermore, the scattered clouds below the cloud base are arranged along several lines approximately 20° and 40° off the nadir, which indicates the discretization artifacts. For the broken cumulus cloud case, the retrieved image shows more pieces of clouds compared to the true image (Figure 4, the middle plate at the bottom). The shape of the cloud patches is not realistic compared to the true image as well. In contrast, the retrieval using the point-function discretization scheme preserves much more features of the original images. The spurious cloud patches disappear in the images retrieved with the point-function discretization scheme for both the stratocumulus and the broken cumulus cases. The geometrical shape of the clouds is also better reproduced with the point-function discretization scheme than that retrieved with the conventional pixel scheme.

For both cloud cases, the retrieval errors corresponding to the point-function discretization scheme are reduced up to 40% compared to those of the pixel scheme, namely, 0.105 gm^{-3} and 0.069 gm^{-3} for the stratocumulus cloud case, 0.076 gm^{-3} and 0.049 gm^{-3} for the broken cumulus cloud case.

4. Concluding remarks

A point-function discretization scheme that approximates continuous distributions based on values over a set of points and predefined linear interpolation functions is developed as a replacement for the conventional pixel scheme. We first demonstrate that the point-function discretization scheme can significantly reduce discretization error compared the

pixel scheme when the same number of unknowns are used for each discretization scheme. The utility of the new point function discretization scheme for ill-posed remote sensing problem is then illustrated with the example of cloud tomography, which involves probing clouds from multiple beams of same or different beam widths and inverting the resulting multi-angular data. The point-function discretization scheme is integrated into a regularization algorithm (i.e., DSCNNLS) to handle the interweaving issue of ill-posedness and discretization found in the practice of cloud tomography. Both the visual inspection and quantitative comparison show that this integrated algorithm substantially improves the tomographic retrieval, reducing the retrieval error by up to 40%.

The point-function discretization scheme indeed has many advantages. With the point-function scheme, the remote sensing retrievals can be sampled at any resolution, while with the pixel scheme they can only be coarsened in quantum jumps. This becomes important for synergetic retrieval from dissimilar remote sensing sensors, each sampling at a different resolution, or even worse the resolution difference being range-dependent due to conical beams; in this case, with the point-function representation, one can sample one instrument at the resolution of the other, or sample both at a new resolution.

Acknowledgments

This research is supported by the DOE Atmosphere Radiation Measurement program under Contract DE-AC02-98CH10886. We thank Dr. Robert McGraw for fruitful discussions on this paper.

References

Ackerman, S.A., O.B. Toon, and P.V. Hobbs (1995): A model for particle microphysics, turbulent mixing, and radiative transfer in the stratocumulus topped marine boundary layer and comparisons with measurements. *J. Atmos. Sci.*, 52, 1204-1236.

Bockmann, C. (2001). Hybrid regularization method for the ill-posed inversion of multiwavelength lidar data in the retrieval of aerosol size distributions. *Applied Optics*, 40,1329-1342.

Delprat-Jannaud, F., and P. Lailly (1993): Ill-posed and well-posed formulations of the reflection travel time tomography problem, *J. Geophys. Res.*, 98, 6589-6605.

Hansen, P.C. (1998): *Rank deficient and ill-posed problems: Numerical aspects of linear inversion*. SIAM, Philadelphia, pp. 247.

Huang, D., Y. Liu, and W. Wiscombe (2008a): Determination of cloud liquid water distribution using 3D cloud tomography. *J. Geophys. Res*., accepted.

Huang, D., Liu, Y., and Wiscombe, W. (2008b): Cloud tomography: role of constraints and a new algorithm. *J. Geophys. Res*., submitted.

Stephens, G., and co-authors (2002): The CloudSat mission and the A-train. *Bull. Amer. Meteor. Soc.*, 83, 1771-1790.

Twomey, S. (1977): *Introduction to the mathematics of inversion in remote sensing inversion and indirect measurements*. Elsevier, Amsterdam, pp. 243.

Twomey, S. (1987): Iterative nonlinear inversion methods for tomographic problems. J. *Atoms. Sci*., 44, 3544-3551.

Scales, J.A., P. Docherty, and A. Gersztenkorn (1990). Regularisation of non-linear inverse problems: Imaging the near-surface weathering layer, *Inverse Problems*, 6, 115-131.

Warner, J., J.F. Drake, and P.R. Krehbiel (1985): Determination of cloud liquid water distribution by inversion of radiometric data. *J. Atmos. Sci. Ocean. Tech*., 2, 293-303.

Warner, J., J.F. Drake, and J.B. Snider (1986): Liquid water distribution obtained from coplanar scanning radiometers. *J. Atmos. Sci. Ocean. Tech*., 3, 542-546.

Figures

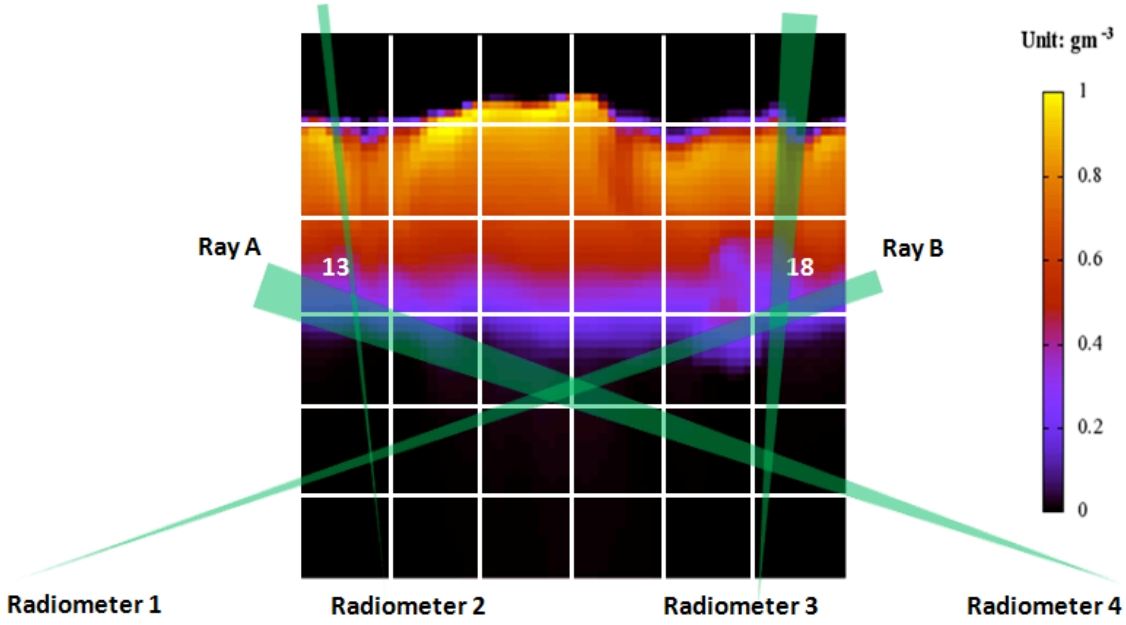

Figure 1. Discretization artifacts of the pixel scheme when using four ground radiometers of different antenna beam widths. The four microwave radiometers are placed on the ground, each 3.33 Km apart. The sampling volume of each radiometer measurement is a cone around the nominate ray and the apex angle of the cone is the beam width. The 5 km wide 1.5 km high domain contains a stratocumulus cloud and is divided into 6x6 pixels. Note that some rays intersect a pixel through its corner, e.g., ray A in pixel 13 and ray B in pixel 18. The brightness temperatures measured along A and B are close to that of a clear sky. The resulting tomographic retrieval would yield very little liquid water in pixels 13 and 18, which is apparently not true.

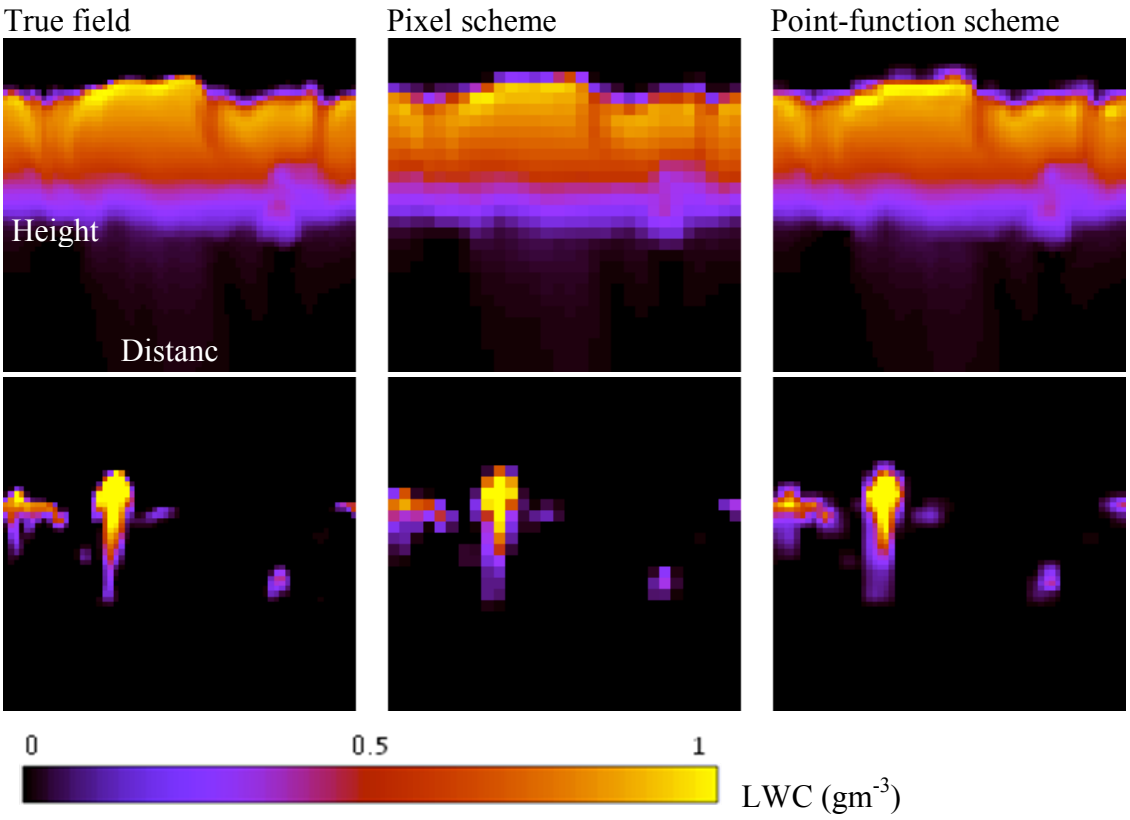

Figure 2. The best approximations to two different cloud cases using the pixel and the point-function discretization schemes with 30x30=900 coefficients (pixels or points): a stratocumulus (top), and a broken cumulus (bottom). The rms errors of the pixel and point-function schemes are respectively 0.055 gm^{-3} and 0.025 gm^{-3} for the stratocumulus cloud. The errors are 0.067 gm^{-3} and 0.040 gm^{-3} for the broken cumulus.

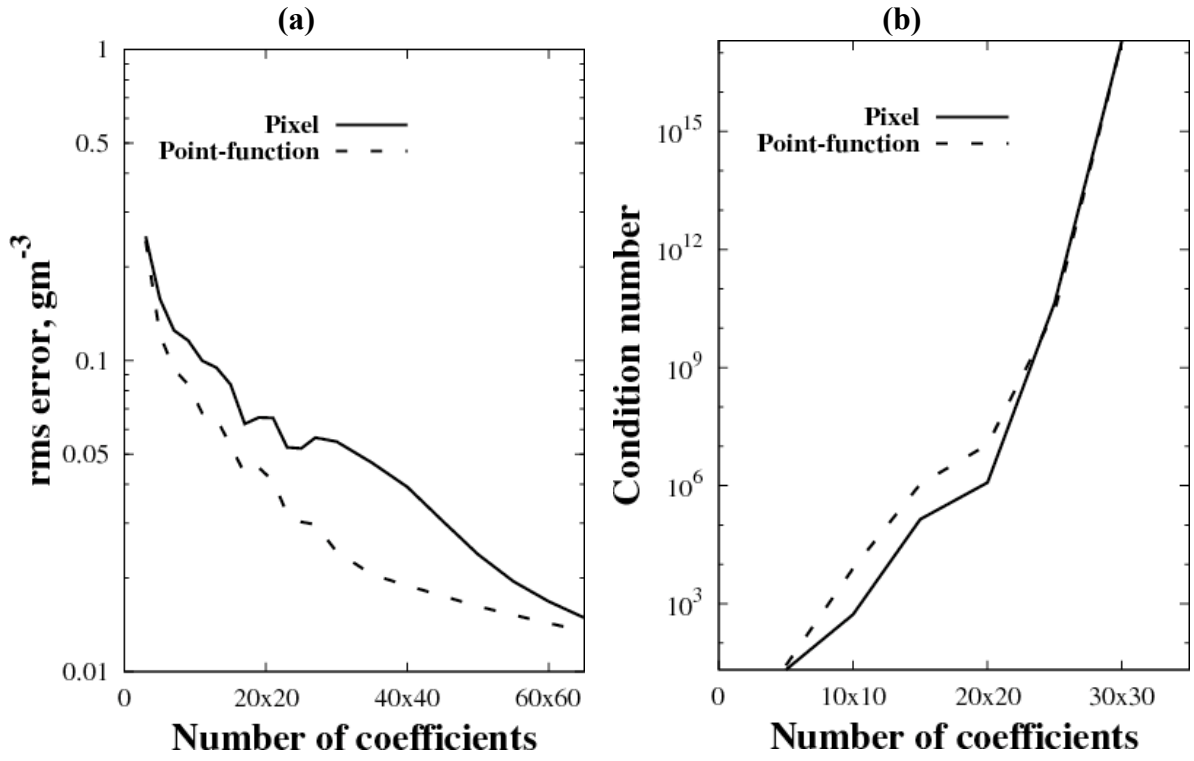

Figure 3. Illustration of the trade-off between discretization error and ill-posedness of the cloud tomography retrieval problem using the stratocumulus cloud shown in Figure 1. Discretization error is quantified by the rms error, while ill-posedness of the retrieval problem is characterized by the condition number of the corresponding kernel matrix **A**. The discretization errors of the pixel and the point-function discretization schemes decrease (a), but the corresponding condition numbers increase (b), with increasing number of pixels or grid points. When the number of points equals the number of pixels, the rms error of the point-function discretization scheme is much lower than that of the pixel scheme, which suggests that the point-function scheme better approximates the stratocumulus cloud than the pixel scheme.

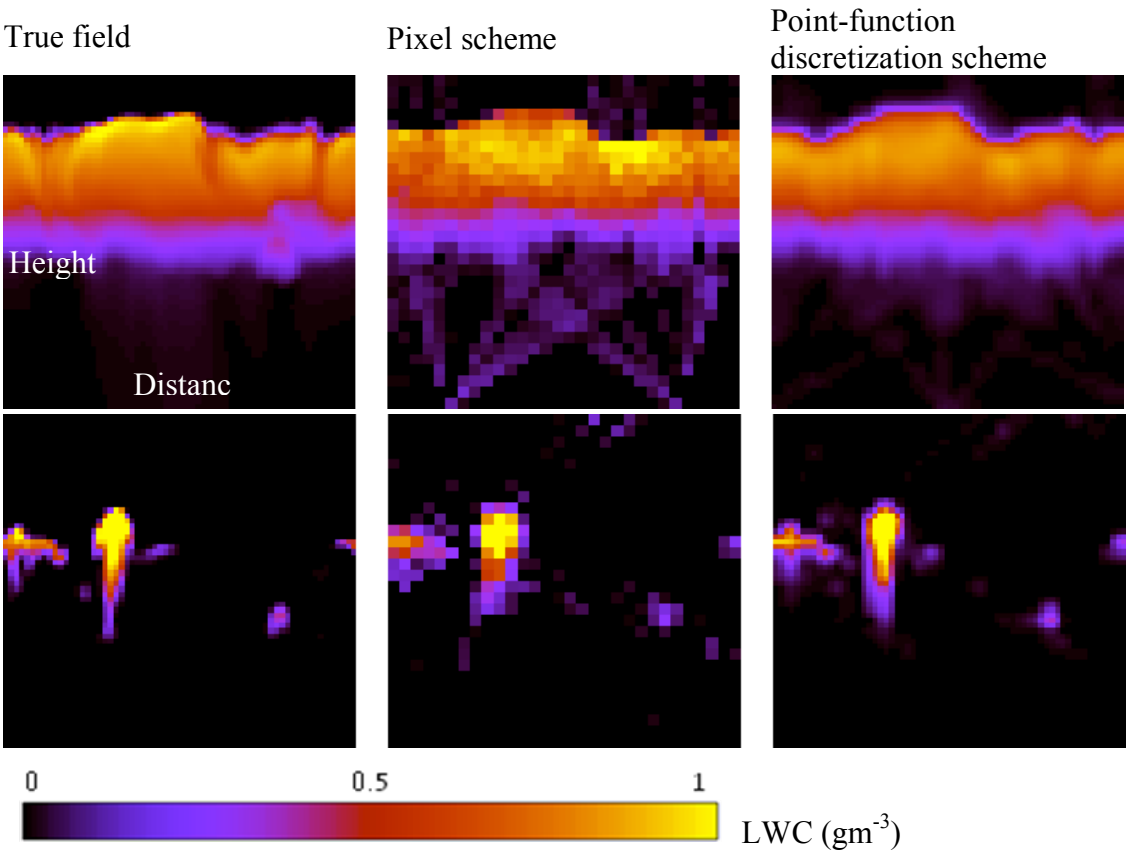

Figure 4. The retrieved images using the pixel and the point-function discretization schemes for the two cloud cases (also shown in Figure 2). The cloud tomography simulations use four ground-based microwave radiometers of 0.3 K noise level and 2-degree beam width to obtain a total number of 900 rays. The Double-side plus Smoothness constrained Non-Negativity Least Squares (DSNNLS) algorithm is used to retrieve the cloud water distributions from the simulated tomographic data. For both discretization schemes, 30x30 = 900 coefficients (pixels or points) are used.